Evaluation of Synchronization Accuracy between High Speed Cameras in Infrared and Visible Spectrums

Senya Polikovsky
for.seny@gmail.com

Yoshinari Kameda
kameda@iit.tsukuba.ac.jp

Yuichi Ohta
ohta@iit.tsukuba.ac.jp

Computer Vision and Image Media Laboratory,
Department of Intelligent Interaction Technologies,
Graduate School of Systems and Information Engineering, University of Tsukuba.

Abstract

Availability and improvements over resent years in infrared and visible spectrum high speed cameras make their use very attractive in computer vision field. In particular, the fusion of these two cameras is utilized for analyzing physiological changes, with durations in milliseconds order. The analysis results strongly depend on the synchronization accuracy of the cameras.

In this paper we present a new approach for evaluating synchronization accuracy between infrared (thermographic) camera and visible spectrum high speed camera. The evaluation is based on angle differences in the specially designed rotating marker on corresponding frames.

We present three algorithms for measuring angle position of the butterfly marker and compare their advantages. We also compare two synchronization strategies on actual devices and show the results.

1. Introduction

Due to improvements in usability of video camera for research purposes and price reduction, there is an increasing number of computer vision research works that base their analysis on the combined video signal from visible spectrum cameras and infrared (IR) spectrum that could be obtained by thermographic cameras. Stephen [1] introduced the use of such signals for human localization and tracking in surveillance videos. Yasuda [2] presented combined camera system for extracting contours of human body for mixed reality applications. Recently, two facial video databases of six basic human emotions using visible spectrum and thermographic cameras were introduced in [3] and [4].

However, all the works mentioned above analyze video signals that were captured by 30 frames per second (fps) cameras and synchronization accuracy issue between the cameras was not discussed.

Our research is focusing on physiological analysis such as rapid facial motions and temperature changes in specific areas of the face and the hands. Visible spectrum camera captures the facial changes and thermographic camera measures changes in the temperature.

Specifically we are interested in measuring: a) timing characteristics of the separate physiological responses and b) time delays between different physiological responses. For this purpose we selected visible spectrum cameras that run at 200fps and Long Wave IR thermographic camera capturing 60fps. For extracting timing information from combined signals we must insure high accuracy in synchronization between the cameras.

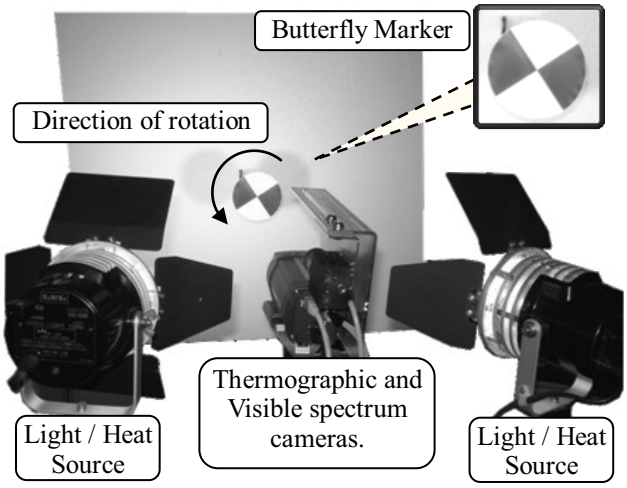

Figure 1. Experiment setup for measuring synchronization accuracy between thermographic camera and visible spectrum high speed cameras. Both cameras simultaneously record the rotational motion of the butterfly marker that is attached to the motor.

Since we need to achieve the synchronization estimation in less than 1/200 seconds without any help of internal triggers between different types of cameras, unfortunately any previously proposed methods cannot meet with our demands.

Modern cameras include variety of synchronization features such as: 1) Frame time stamp that comes from external or internal clock. 2) Strobe output pulse signals from camera that corresponds to the shutter operation. 3) General Purpose Input/Output (GPIO) ports that can be controlled externally and their logical state is attached to every frame in the video (for example it can be used for marking relevant frames for future analysis). 4) External control over the shutter operation.

In addition, some protocol based synchronization can be found, for example FirePRO introduced by PointGray company supports automatic synchronization between linked cameras within 12 microseconds. However, most of the protocols in their standard implementation such as USB, Camera Link, FireWire, GiG are not including synchronization option.

Users can choose different synchronization strategies, applying one or combination of strategies. However, no matter which synchronization strategy is chosen it is

important to have the ability to evaluate the synchronization accuracy in applications where high speed cameras are used.

This paper proposes a new approach for synchronization accuracy evaluation between high speed cameras in infrared and visible spectrums.

The rest of the paper is organized as follows: In section 2 we define experimental setup. In section 3, three algorithms for marker angle estimation are presented. Section 4 presents our experiment results. Finally, we conclude the paper in Section 5 and point to future work.

2. Synchronization Evaluation Approach

The straightforward approach for measuring camera synchronization is done by recording an event over time with two (or more) cameras, and by extracting the differences in corresponding video frames.

When all the cameras in the system are working in visible or near-infrared spectrums, such event can be represented by 7-segment high speed clock counter. In this case the counter pace is defined by the shutter speed of the cameras. Using the 7-sigment counter by looking at the captured counter display in corresponding frames the delay can be calculated. For more automatic procedure it is possible to use LED board such as [5]. However, if thermographic cameras of Middle Wave Infrared (MWIR) or Long Wave Infrared (LWIR) spectrums are part of the system the above approaches are not applicable, as the LEDs light cannot be observable by these cameras.

For thermographic cameras an event should involve temperature change that could be spotted in the same time by thermographic and visible spectrum cameras. Such event could be mechanical motion. The analysis of the linear motion between the frames requires calibration procedure between the cameras. As for the rotational motion analysis, it is less sensitive to the calibration and can be easily implemented by using standard motor or electrical fan.

In our setup, we attached a "butterfly" marker (see Figure 1) to the voltage speed control motor. By knowing the angular speed of the motor **w** and measuring the difference in rotational angle between corresponding frames **Δα** we can calculate time delay **ΔT** by formula (1)

$$\Delta T = {}^{\Delta\alpha}/_{W} \tag{1}$$

For getting the temperature differences the marker is illuminated with strong light that functions as stable heat source. The black color areas on the printed marker accumulate more heat than the white areas. This difference can be clearly seen on thermographic camera images. In addition, a strong light source allows both shortening the shutter speed of the visual light cameras and making sharper video images. In the next section, we will describe the angle estimation algorithms.

3. Angle Estimation from Butterfly Marker

This section presents three algorithms for measuring angle position of the "butterfly" marker. The three algorithms are: 1) Image moment, 2) circle frequency filter, and 3) maximization of the intensity ratio between "black" and "white" areas of the marker.

In figure 2 we present video frames of the marker during the rotational motion. As expected the frame taken by high speed camera is clear and sharp. However we can see that the thermographic camera frame suffers from blur and some asymmetry in the marker shape.

Our assumptions for all the algorithms are:

1.) Cameras are placed perpendicularly to the marker surface so the marker shape stays circular. 2.) The location of the marker is stable during entire video. 3.) The axis of the rotation is at the center of the marker.

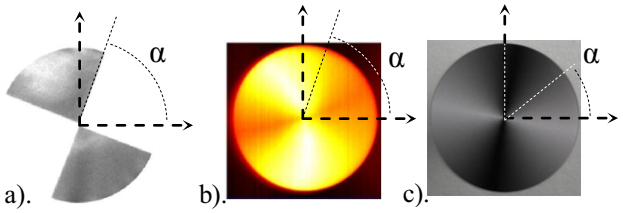

Figure 2. Video frames of the marker and the rotational angles. a). Visible spectrum camera (200fps, 1ms shutter speed) under strong illumination. b). Thermographic camera (60fps, 12ms shutter speed). c.) Visible spectrum camera (30fps, 15ms shutter speed)

3.1. Image Moment

This is simple algorithm based on the fundamental work[6]. Equation (2) presents "raw image moment" $\mathbf{M_{ij}}$ of order i and j, and **I(x,y)** is a grayscale image. $\bar{x}$ and $\bar{y}$ are the components of the centroid defined by equation (3). The orientation angle **α** corresponds to the major axis of the image intensity given by equation (4).

$$M_{ij} = \sum_x \sum_y x^i y^j I(x,y) \tag{2}$$

$$\bar{x} = \frac{M_{10}}{M_{00}}, \quad \bar{y} = \frac{M_{01}}{M_{00}} \tag{3}$$

$$\alpha = \frac{1}{2}\, tan^{-1}\left(\frac{2(M_{11}/M_{00} - \bar{x}\bar{y})}{(M_{20}/M_{00} - \bar{x}^2) - (M_{02}/M_{00} - \bar{y}^2)}\right) \tag{4}$$

In this approach we introduce one more assumption; the symmetry of the marker is preserved in the image. The introduction of the threshold value for getting binary image can solve the problem of non monotonic intensity in the "black" area of the marker. But asymmetrical and blurry images cannot be processed by the threshold. Further improvement can be achieved by applying a ring shaped mask for excluding undesired areas in the marker image.

For sharp and monotonic images this approach gives the best results (see Figure 2. a.).

3.2. Circle Frequency Filter

The intensity value on perimeters of any circle that share the same center with the butterfly marker forms a periodic wave with spatial frequency of two (see Figure. 3). First, by using Midpoint circle algorithm [7] for speed-up, we map pixel value on the perimeter of the circle of radius r at 2D **I(x,y)** onto 1D **f(k)**. By applying Fourier transform of equation (5) on **f(k)** we can calculate magnitude and phase for any spectrum frequency **p**. The important characteristic of this filter is that, its phase shift

output result is identical to the rotational angle of the image. It can be calculated by equation (6). The final angle estimation is done based on 20 different radiuses.

$$Y_p = \sum_{k=0}^{N-1} f(k)\left(\cos\left(2\pi\frac{kp}{N}\right) + i\sin\left(2\pi\frac{kp}{N}\right)\right) \quad (5)$$

$$\alpha_p = \tan^{-1}\left(\frac{\sum_{k=0}^{N-1} f(k)\sin\left(2\pi\frac{kp}{N}\right)}{\sum_{k=0}^{N-1} f(k)\cos\left(2\pi\frac{kp}{N}\right)}\right), p = 2 \quad (6)$$

The algorithm can be also considered as a filter for removing high frequency noise.

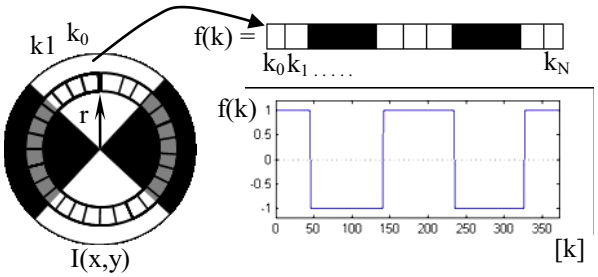

Figure 3. Circle filter maps pixel value from I(x,y) to f(k), starting from upper point in counter-clockwise direction. Then the phase angle of f(k) is calculated by equation (6).

3.3. "Black" and "White" Intensity Ratio Maximization

We know that the 50% of the pixels in the video frame inside the marker area corresponds to "black" area, and 50% correspond to "white" area. In addition, we take in consideration the position of each of the areas.

We define function **g(α, I)** where input parameter **α** represents rotational angle of the marker in the image **I(x,y)**. This function returns the sum of the intensity of all the pixels in the "black" area. Function **h(α, I)** is defined in the same way for "white" area, see equation (7) . In equation (8), we search angle **α** that will maximize the accumulated intensity ratio between **g** and **h** to fit the "black" and "white" areas appropriately.

$$g(\alpha, I) = \sum_{x,y \in \text{black area}} I(x,y)$$
$$h(\alpha, I) = \sum_{x,y \in \text{white area}} I(x,y) \quad (7)$$

$$\text{argmax}_{\alpha\in(0,\pi)} \frac{g(\alpha, I)}{h(\alpha, I)} \quad (8)$$

In our implementation, we rely on the fact that the pixels on the radius line from the center of the marker belong to the same area. First, we sum all the pixels on the radius lines in the direction of the discrete angle **θ**. We do it by applying polar transformation on **I(x, y)** to **P(r, θ)**, placing the origin on the center of the marker, and then counting all the columns in image **P(r, θ)** to obtain **F(θ)**. Note that pixels from both ends of the radius line are not counted (see Figure 4). By **F(θ)** it is easy to sum all the pixels from "black" and "white" areas and search for the maximum ratio.

It is possible to control the accuracy level of the allgorithem by setting different division of the discrete angle **θ.**

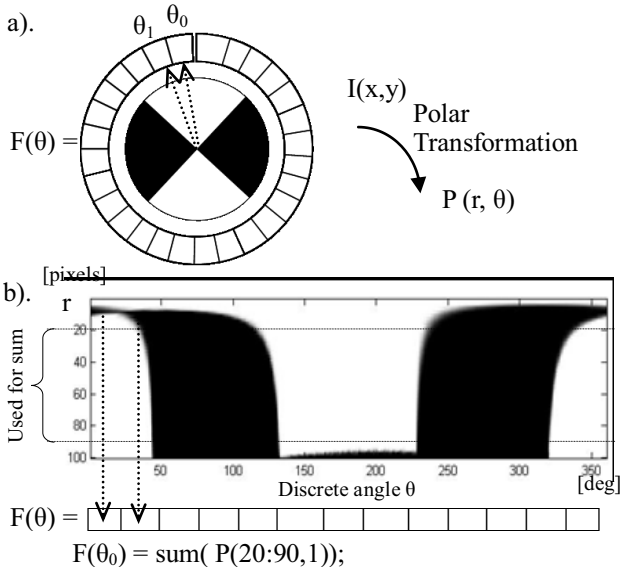

Figure 4: a) Ilustrated F(θ) as the sum of all the pixels on the radius line from the center of the marker, parameter θ defined as a discrete value. b) Ilustrated the polar transformation used in the implementation of functions g() and h() in equation (7).

3.4. Comparison of The Algorithms

In figure 5, we present results of applying the proposed three algorithms on synthetic frames and real frames from a visible spectrum camera and thermographic camera. Synthetic frames of the marker were generated by computer graphics. Examples of real marker images are shown in figure 2. For synthetic data the image moment approach is the most stable. However, based on the assumption that the motor speed is constant, our tests show that intensity ratio maximization approach tends to be more stable for high speed visible light frames and the circle frequency filter approach shows better stability with thermographic frames.

4. Synchronization Evaluation Experiment

This section describes the experiment on synchronization evaluation between visible spectrum and

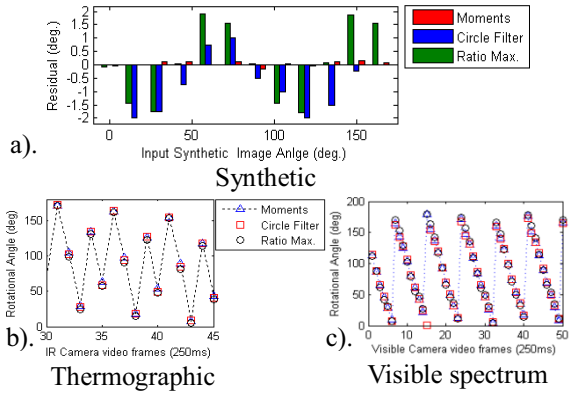

Figure 3. Results of angle estimation on a) synthetic frames, b) real thermographic camera frames, c) real visible spectrum frames.

thermographic cameras.

For capturing visible spectrum (denoted by VS) we used is Grasshopper from PointGrey at 200 fps, 1.0 millisecond shutter speed with IEEE 1394b (FireWire) protocol. Thermographic camera (denoted by IR) is LWIR A325 from FLIR running at 60 fps, 12.0 millisecond shutter speed with Gig Ethernet protocol. Both of the cameras are capable to attach internal timestamp, frame ID and logical state of external IN and OUT ports for every frame. The Grasshopper camera has external shutter control option but it is limited to support maximum of 180 fps. Thermographic camera does not have this function.

In this experiment we compared two synchronization strategies using the experimental setup as shown in figure 1. First video of the marker with 12RMS are recorded simultaneously by both cameras. Second, corresponding frames are coupled. Finally, time difference at each frame pair is calculated.

We evaluate the synchronization during 5 minutes video sequence, as this is the maximum length that we use for our physiological analysis experiments.

4.1. Synchronization by First Frame

The first synchronization is simple. We use I/O ports IR-IN1 and VS-IN1 in both cameras for indicating the first corresponding pairs by setting these port values to "1" simultaneously. Then, by using timestamp of frames we matched frames in video sequences.

The first captured frame that was fully aligned with the frame from other sequence is considered to be corresponding pair. For example in Figure 6 the corresponding frames are: IR=1 to VS=1, IR=2 to VS=5, IR=3 to VS=8.

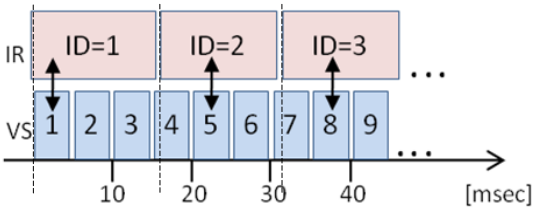

Figure 4. Logic behind the matching process of corresponding frames between IR and VS video sequences. The arrows represent the corresponding frames.

4.2. Synchronization by Strobe Pulse

The starting frames are located similar to the previous strategy. In addition, we configure VS-OUT1 port to strobe output signal. This is build-in option of Grasshopper camera. The strobe signal was configured to send one pulse at every 200 frames (once per second.) The signal is connected to IR-IN2 of the A325 camera. As a result, the corresponding frames can be confirmed once per second.

The evaluation results of both strategies are presented in figure 7.

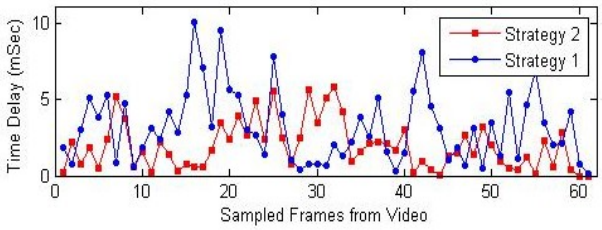

Figure 5. Time delay between last 60 frame pairs of IR and VS of 5 min test video. Strategy 2 improves the synchronization accuracy

5. Results and Conclusion

In this paper we presented a new approach for evaluating synchronization accuracy between high speed visible spectrum and thermographic cameras.

Our approach is based on comparing rotational angle of the butterfly marker between the corresponding video frames. The marker is attached to a small electric motor of stable rotational speed. If the rotational speed is given it is possible to calculate the exact time delay between the frames.

We presented three different algorithms for measuring rotational angle from the butterfly marker images. The proper algorithm should be chosen based on the quality of the video we can obtain. We also presented the evaluation results of two synchronization strategies.

As for the next step, we plan to compare the proposed algorithms of rotational angle measurement by ground truth data using a motor that can report its rotational angle in real time.

The limitation of our approach is its' inability to recognize the delay of one or more full cycles.

All the Matlab programs of this paper are available at the author's homepage. We hope that this work will encourage other researchers to tackle synchronization evaluation problem for achieving better and more accurate sensors fusion.

References

[1] S. Krotosky, and M. Trivedi, "Registration of Multimodal Imagery with Occluding Objects using Mutual Information", *Lecture Notes in Computer Science: Object Tracking and Classification in and Beyond the Visible Spectrum*, 2007.

[2] K. Yasuda, T. Naemura, and H. Harashima, "Thermo-Key: Human Region Segmentation from Video," *IEEE Computer Graphics and Applications*, pp. 26-30, 2004.

[3] T. Marks, J. Hershey, and J. Movellan, "Tracking Motion, Deformation, and Texture Using Conditionally Gaussian Processes," *IEEE Trans. Pattern Analysis and Machine Intelligence*, pp. 348-363, 2010.

[4] S. Wang, et el. "A Natural Visible and Infrared Facial Expression Database for Expression Recognition and Emotion Inference, " *Multimedia*, vol.12, no.7, pp.682-691, 2010.

[5] G. Litos, X. Zabulis, and G. Triantafyllidis, "Synchronous Image Acquisition based on Network Synchronization," *Conference on Computer Vision and Pattern Recognition Workshop*, pp. 167, 2006.

[6] M. K. Hu, "Visual Pattern Recognition by Moment Invariants," *IRE Trans. Info. Theory*, vol. IT-8, pp.179–187, 1962.

[7] M. Pitteway, "Algorithm for Drawing Ellipses or Hyperbolae with a Digital Plotter," *Computer Journal*, vol.10, no.3, pp. 282-289, 1967.